

# Chapter 1

## Near-Field Excitation Dynamics in Molecules: Nonuniform Light-Matter Interaction Theory Beyond a Dipole Approximation

Katsuyuki Nobusada

**Abstract** We have presented near-field excitation dynamics in molecules beyond diffraction limit of the incident visible laser field. A generalized theoretical description of a light-matter interaction taking account of nonuniformity of the light due to its intensity gradient has been developed on the basis of the multipolar Hamiltonian. The computations are demonstrated in high-harmonic generation spectra of a linear chain molecule of dicyanodiacetylene, NC<sub>6</sub>N and also in optical forces induced by a near-field for a 1 nm-sized metal particle mimicked by a jellium model and for C<sub>60</sub>.

### 1.1 Introduction

Optical response of molecules is undoubtedly essential for understanding their physicochemical properties. For example, UV-vis light is used to study electronic states of molecules, far-infrared light for molecular vibrations, microwave for molecular rotations and so forth. In these optical responses, wavelengths of the lights are usually considered to be much longer than molecular sizes. Thus, a target molecule is well approximated by a point dipole and the dipole feels an almost uniform electromagnetic field. This condition underlies the conventional dipole approximation. Furthermore, light is an external field to excite molecules and its wavelength is definitely determined by an apparatus condition. Since spatial resolution of spectroscopy is limited by the wavelength of the incident light, it is impossible to gain molecular properties in a local region shorter than the wavelength, i.e., diffraction limit. The conventional optical response mentioned above is referred here to as a far-field and matter interaction.

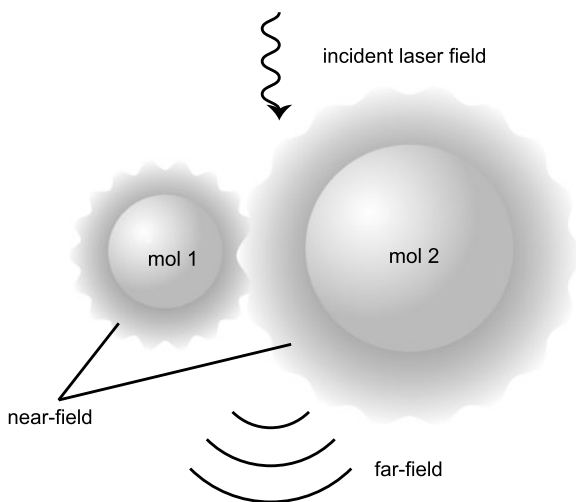
However, recent development of nanofabrication and nano-optical techniques requires a more general optical response theory for the following reasons. (We note that the light is considered here to be a classical wave determined by the Maxwell equations, although it should be treated in a narrow sense by resorting to the quantum electrodynamics theory.) When noninteracting or weakly-interacting nanopar-

---

K. Nobusada (✉)

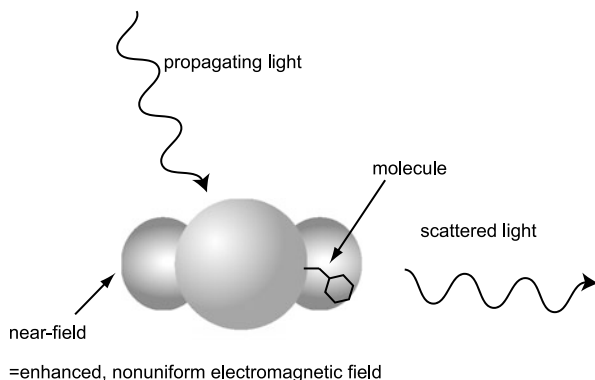
Department of Theoretical and Computational Molecular Science, Institute for Molecular Science, 38 Myodaiji-Nishigonaka, Okazaki, Aichi 444-8585, Japan  
e-mail: [nobusada@ims.ac.jp](mailto:nobusada@ims.ac.jp)

**Fig. 1.1** Schematic diagram of a near-field and a far-field from distant molecules 1 and 2 in the presence of an incident laser field



ticles are irradiated by an incident laser pulse, electric dipoles are induced in the nanoparticles. The induced dipoles generate local electric fields, in addition to far-fields, around the nanoparticles and then the adjacent particles can interact with each other through the local fields. This local field is often referred to as a near-field in contrast to a far-field. Figure 1.1 shows a schematic diagram of a near-field and a far-field from molecules irradiated by the incident laser field. The near-field interaction is significantly different from the far-field interaction [1–7]. If the near-field irradiates adjacent particles, the new near-field is subsequently generated around the particles. The new near-field recursively irradiates other particles and these sequential light-matter interactions between the particles persist self-consistently. As a result of the self-consistent interaction, an enhanced electric field, which is closely related to surface enhanced Raman scattering (SERS) [8–10], appears around the particles. A schematic diagram of SERS of a metallic-nanoparticle and molecule system is depicted in Fig. 1.2. Such locally enhanced electric fields have been observed experimentally [11] and intensively simulated in an effort to understand mechanisms of SERS by solving the Maxwell equations [12, 13]. SERS has currently attracted much attention in a wide range of research fields, and there is interest in both achieving a fundamental understanding of SERS itself and also in applications to engineering, biology, medical science, and pharmacology [14–16]. For example, a large enhancement in Raman intensity is expected to realize single-molecule detection [17, 18]. SERS effects are also thought to be applicable for developing ultrasensitive chemical sensors or imaging tools, especially for biomolecules [19, 20]. Second, as shown in Fig. 1.1 the near-field is a non-propagating wave rapidly decaying from the surface of a radiating-source particle, that is, the spatial variation of the near-field is of the same order of magnitude as the particle size. Thus, the near-field interaction occurs in a narrow region comparable with the size of the particle. In other words, the near-field and matter interaction, in sharp contrast to the far-field interaction, is a nonuniform one and the spatial structure of the near-field plays a crucial role.

**Fig. 1.2** SERS is schematically illustrated. The *center particle* and the *right and left circles* represent a metallic nanoparticle and a near-field interaction, respectively. A molecule on the surface of the nanoparticle is exposed to the near-field and scatters the light



This means that the near-field overcomes the diffraction limit and gives in principle information about molecular properties associated with local structures even of 1-nm-sized nanoparticles or molecules. Conversely, those great advantages of the near-field interaction, that is, the self-consistency and the nonuniformity, require to describe light-matter interactions in a more general way.

Basic frameworks of optical response taking account of the full nonuniform and self-consistent light-matter interactions have so far been developed [21–23]. Although the studies were made in various molecular or nanostructure systems at different levels of theory, the authors drew essentially the same conclusion that those full light-matter interactions have a great influence on optical properties of the systems. Very recently, to confirm the importance of the full light-matter interactions in optical response, explicit computational demonstrations have been carried out in more specific nanosystems such as nanocrystals, semiconductor quantum dots, nanoparticles, and molecular compounds [12, 13, 24–28]. Every study clearly showed significant effects of the full light-matter interactions beyond the dipole approximation. An electric field enhancement due to the self-consistent light-matter interaction is a key ingredient in understanding a mechanism of SERS and its computations have been intensively demonstrated as mentioned above [12, 13]. Multipole effects concerning the nonuniform light-matter interaction were discussed in nanoparticles [25, 27], and molecular compounds [24]. Furthermore, the self-consistent and nonuniform light-matter interactions were verified in detail to play a crucial role in optical response to localized light fields generated between nanostructures [27, 28]. These explicit demonstrations have usually been done for model systems, simplifying the electronic structures of target nanostructures, for example, the nanostructures were assumed to be dielectric particles or their optical susceptibilities were given in advance. This is partly because it is computationally highly demanding to fully quantum-mechanically solve electron dynamics of the target nanosystems coupled with the electromagnetic field dynamics, in particular almost impossible for real nanostructures in a 1 nm size or more. Nevertheless, in molecular science, it is essential to calculate optical properties associated with details of electronic structures, such as geometric structures, bond characters, charge distribution, and electron correlation of target nanostructures. To describe optical response

of 1-nm-sized molecules, we split the full-light-matter interaction into the issues of self-consistency and nonuniformity. We first consider the nonuniform light-matter interaction as an initial step and leave the self-consistent interaction (i.e., solving the Maxwell-Schrödinger coupled equation) for the next. Here, a first-principles approach to treat a nonuniform light-matter interaction in real molecular systems is developed. We place special emphasis on obtaining full quantum-mechanical solutions of electron dynamics under the near-field (i.e., local field) to elucidate the nonuniform light-matter interaction at the level of molecular theory.

The conventional optical response theory is usually formulated starting from the minimal coupling Hamiltonian, and the formulation often relies on the dipole approximation. In contrast, we develop a more general theory without the dipole approximation, on the basis of the multipolar Hamiltonian derived from the minimal coupling Hamiltonian by a canonical transformation [22, 29–31]. The light-matter interaction in the multipolar Hamiltonian is described in terms of the space integral of an inner product of polarization and an electric field, whereas the minimal coupling Hamiltonian uses momentum and vector potential. The last two variables are rather inconvenient for practical calculations. Noteworthy is the fact that in the multipolar Hamiltonian approach the polarization in the integral can be treated entirely without any approximations. This means that infinite orders of multipole moments are taken into account. Therefore, the present approach is a generalization of the conventional optical response theory with the dipole approximation.

To investigate optical properties of real molecules, explicit time-evolution of electron dynamics should be solved. To this end, we have incorporated our optical response theory with the nonuniform light-matter interaction into our developed electron-dynamics simulation approach in real space [32–35] based on time-dependent density functional theory (TDDFT). The integrated TDDFT approach has been applied to and computationally solved for a test molecular system of dicyanodiacetylene (NC<sub>6</sub>N) as an example, to elucidate the electron dynamics of 1-nm-sized molecules induced by the nonuniform near-field. Specifically, high-harmonic-generation (HHG) spectra induced by the near-field excitation are compared with those excited under the uniform light-matter interaction. The near-field excitation dynamics is also computationally demonstrated in optical forces exerted in a 1 nm-sized metal particle mimicked by a jellium model and in C<sub>60</sub>.

## 1.2 Theory

### 1.2.1 Multipolar Hamiltonian

Electron dynamics in a molecule interacting with electromagnetic field is generally described by the time-dependent Schrödinger equation based on minimal coupling Hamiltonian consisting of vector potential  $A$  and scalar potential  $\phi$ . Instead of using the minimal coupling Hamiltonian, however, we start our theoretical formulation from the multipolar Hamiltonian to include full spatial variation of an electric

field for the nonuniform light-matter interaction. The multipolar Hamiltonian can be derived from the minimal coupling Hamiltonian through a canonical transformation [29, 30]. It should be noted that in this study the electric field is considered to be a classical value and any magnetic interactions are neglected. The inter-molecular distances are assumed to be large enough so that their electronic wavefunctions do not overlap. The multipolar Hamiltonian of non-overlapping molecules interacting with an electric field is then obtained as [31]

$$\hat{H} = \hat{H}_{\text{mol}} + \hat{V}_{\text{inter}} - \int d\mathbf{r} \hat{\mathbf{P}}(\mathbf{r}) \cdot \mathbf{E}^{\perp}(\mathbf{r}, t), \quad (1.1)$$

where  $\hat{H}_{\text{mol}}$  is the Hamiltonian of the molecules and  $\hat{V}_{\text{inter}}$  is the static intermolecular Coulomb interaction.  $\hat{\mathbf{P}}(\mathbf{r}) = \sum_i \hat{\mathbf{P}}_i(\mathbf{r})$  is the total polarization operator of the system with  $\hat{\mathbf{P}}_i(\mathbf{r})$  being the polarization operator of the molecule  $i$ .  $\mathbf{E}^{\perp}(\mathbf{r}, t)$  is the transverse part of the electric field written in the form of

$$\mathbf{E}^{\perp}(\mathbf{r}, t) = \mathbf{E}_{\text{laser}}^{\perp}(\mathbf{r}, t) + \sum_j \mathbf{E}_j^{\perp}(\mathbf{r}, t), \quad (1.2)$$

where  $\mathbf{E}_{\text{laser}}^{\perp}(\mathbf{r}, t)$  is an incident laser field and  $\mathbf{E}_j^{\perp}(\mathbf{r}, t)$  is the electric field radiated from the  $j$ -th molecule obtained by solving the Maxwell equations using  $\mathbf{P}_j^{\perp}(\mathbf{r}', t - |\mathbf{r} - \mathbf{r}'|/c)$  as a source with  $c$  being the speed of light. The static intermolecular Coulomb interaction is given by

$$\hat{V}_{\text{inter}} = \frac{1}{\epsilon_0} \sum_{i < j} \int d\mathbf{r} \hat{\mathbf{P}}_i^{\parallel}(\mathbf{r}) \cdot \hat{\mathbf{P}}_j^{\parallel}(\mathbf{r}), \quad (1.3)$$

where  $\hat{\mathbf{P}}_i^{\parallel}(\mathbf{r})$  is the longitudinal part of  $\hat{\mathbf{P}}_i(\mathbf{r})$ . Then, Eq. (1.1) is rewritten as

$$\hat{H} = \hat{H}_{\text{mol}} + \frac{1}{\epsilon_0} \sum_{i < j} \int d\mathbf{r} \hat{\mathbf{P}}_i^{\parallel}(\mathbf{r}) \cdot \hat{\mathbf{P}}_j^{\parallel}(\mathbf{r}) - \sum_i \int d\mathbf{r} \hat{\mathbf{P}}_i(\mathbf{r}) \cdot \mathbf{E}^{\perp}(\mathbf{r}, t). \quad (1.4)$$

The explicit form of  $\hat{\mathbf{P}}_i(\mathbf{r})$  is [29–31]

$$\hat{\mathbf{P}}_i(\mathbf{r}) = \sum_{\alpha} e_{\alpha} (\hat{\mathbf{q}}_{\alpha} - \mathbf{R}_i) \int_0^1 d\lambda \delta(\mathbf{r} - \mathbf{R}_i - \lambda(\hat{\mathbf{q}}_{\alpha} - \mathbf{R}_i)), \quad (1.5)$$

where  $e_{\alpha}$  and  $\hat{\mathbf{q}}_{\alpha}$  are the charge and the position operator of the  $\alpha$ -th electron in the molecule  $i$ , respectively, and  $\mathbf{R}_i$  is the center of mass of the molecule. The integration in Eq. (1.5) with respect to  $\lambda$  is introduced to express the polarization in such a compact form, instead of using multipoles explicitly.

We address here the relation between our optical response formula and the conventional approach based on a multipole expansion method. Eq. (1.5) can be expanded in a Taylor series leading to the dipole, quadrupole, octapole, and higher-

order multipole terms. The present formulation is thus a generalization of the conventional optical response theory with the dipole approximation. Applying the Taylor expansion to Eq. (1.5) and integrating the resulting equation with respect to  $\lambda$ , we obtain

$$\begin{aligned}
 \int d\mathbf{r} \hat{\mathbf{P}}(\mathbf{r}) \cdot \mathbf{E}^\perp(\mathbf{r}, t) &= \left( \sum_{\alpha} e_{\alpha} (\hat{\mathbf{q}}_{\alpha} - \mathbf{R})_i \right) \cdot \mathbf{E}_i^\perp(\mathbf{R}, t) \\
 &\quad - \left( \frac{1}{2!} \sum_{\alpha} e_{\alpha} (\hat{\mathbf{q}}_{\alpha} - \mathbf{R})_i (\hat{\mathbf{q}}_{\alpha} - \mathbf{R})_j \right) \nabla_i \mathbf{E}_j^\perp(\mathbf{R}, t) \\
 &\quad + \left( \frac{1}{3!} \sum_{\alpha} e_{\alpha} (\hat{\mathbf{q}}_{\alpha} - \mathbf{R})_i (\hat{\mathbf{q}}_{\alpha} - \mathbf{R})_j (\hat{\mathbf{q}}_{\alpha} - \mathbf{R})_k \right) \\
 &\quad \times \nabla_i \nabla_j \mathbf{E}_k^\perp(\mathbf{R}, t) \cdots \\
 &\equiv \hat{\mu}_i \mathbf{E}_i^\perp + \hat{Q}_{ij} \nabla_i \mathbf{E}_j^\perp + \hat{O}_{ijk} \nabla_i \nabla_j \mathbf{E}_k^\perp \cdots, \quad (1.6)
 \end{aligned}$$

where  $\hat{\mu}_i$ ,  $\hat{Q}_{ij}$ , and  $\hat{O}_{ijk}$  represent the dipole, quadrupole, and octapole moments of a molecule, respectively, and the indexes denote their ( $x, y, z$ ) tensorial components. These moments are defined at the molecular center  $\mathbf{R}$ .  $\nabla_i$  is the gradient operator along the  $i$ -th direction and acts on the electric field. We here use a contraction of  $x_i y_i = \sum_i x_i y_i$ . The dipole moment couples with the field itself, the quadrupole with the first derivative of the field, and the octapole with the second derivative of the field, and so forth. If an electric field varies slowly over a whole spatial region, the optical response can be reasonably described by only the first term of this expansion (i.e., the dipole approximation). The higher multipole effect is taken into account by including the higher terms of Eq. (1.6). However, the near-field interaction requires an infinite number of terms in the expansion because of its nonuniform spatial structure. Therefore, we use Eq. (1.5) as is, without performing the Taylor expansion of the polarization.

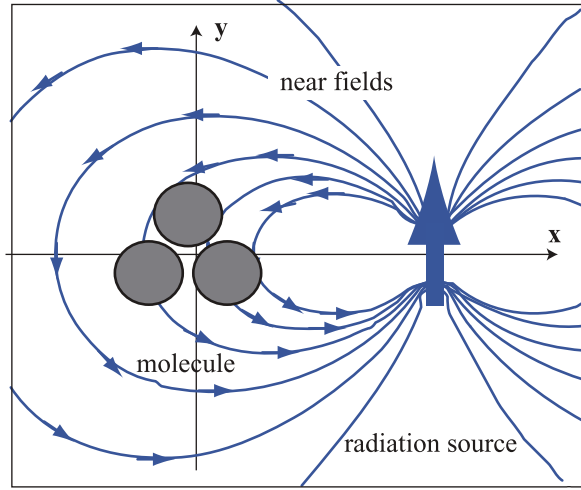
### 1.2.2 A Molecule Interacting with a Nonuniform Near-Field

In the previous section, we have formulated a general theory of the light-matter interaction. To demonstrate the electron dynamics in molecules interacting with a near-field, we first introduce a theoretical model consisting of two molecules irradiated by a laser light. The multipolar Hamiltonian Eq. (1.4) is rewritten for such a model system by

$$\hat{H}_{\text{mol}} + \frac{1}{\varepsilon_0} \int d\mathbf{r} \hat{\mathbf{P}}_1^\parallel(\mathbf{r}) \cdot \hat{\mathbf{P}}_2^\parallel(\mathbf{r}) - \int d\mathbf{r} (\hat{\mathbf{P}}_1(\mathbf{r}) + \hat{\mathbf{P}}_2(\mathbf{r})) \cdot \mathbf{E}^\perp(\mathbf{r}, t). \quad (1.7)$$

As mentioned in the beginning of this article, the near-field is a non-propagating local field around nanostructures, generated in the presence of laser irradiation.

**Fig. 1.3** Nonuniform light-matter interaction model derived from the near-field excitation process shown in Fig. 1.1. The molecule 2 is considered to be a radiation source approximated by an oscillating dipole. The near-fields, i.e., nonuniform electric fields, radiated from the oscillating dipole are shown in the *thin curves with arrows*



Although the near-field should be given by solving the Maxwell equations (or by resorting to quantum electrodynamics theory in a narrow sense), it is reasonably approximated by the short-range term of an oscillating dipole radiation [6, 36]. Then, the theoretical model given by Eq. (1.7) can be further simplified as follows. We discuss here optical response of the molecule 1 interacting only with the near-field radiated from the molecule 2, in which the molecule 2 is considered to be an oscillating dipole as shown in Fig. 1.3. This approximation means that the material Hamiltonian of the molecule 1 is solved quantum mechanically, whereas the molecule 2 is assumed to be a classical dielectric merely as a radiation source. Furthermore, we neglect the near-field induced around the molecule 1, which might affect the dielectric molecule 2 (i.e., the self-consistent effect) when the molecule 1 is electronically excited in its resonance state [27]. Since we focus on roles of the nonuniform electric field in electronic excitation of a molecule, the near-field frequency is chosen so that the resonance excitation does not occur principally. In addition, if the molecule 1 is smaller than the molecule 2, its induced polarization is also relatively smaller than that of the molecule 2. Thus, it is reasonable for the moment to neglect the induced near-field around the molecule 1. In other words, our light-matter interaction model is expected to be useful for studies about spatially-resolved local spectroscopy taking advantage of the nonuniform light-matter interaction in real molecules, because radiations from target molecules are usually weak compared to those of probe tips. For these reasons, the self-consistent effect is left for the future investigation. The incident laser field  $E_{\text{laser}}^{\perp}$  in the third term of Eq. (1.7) is required to induce the polarization associated with the oscillating dipole in the molecule 2. From our preliminary calculations, however, the incident field was found to be less important for the light-matter interaction in the near-field region because the intensity of the induced near-field is larger than that of the incident field. As a result, the electron dynamics in this region is qualitatively unaffected even if the incident laser field is neglected.

Under these conditions, Eq. (1.7) can be reduced to the form of

$$\begin{aligned} \hat{H}_{\text{mol}} - \int d\mathbf{r} \hat{\mathbf{P}}_1^{\parallel}(\mathbf{r}) \cdot \tilde{\mathbf{E}}_2^{\parallel}(\mathbf{r}, t) \\ - \int d\mathbf{r} (\hat{\mathbf{P}}_1(\mathbf{r}) + \hat{\mathbf{P}}_2(\mathbf{r})) \cdot (\tilde{\mathbf{E}}_1^{\perp}(\mathbf{r}, t) + \tilde{\mathbf{E}}_2^{\perp}(\mathbf{r}, t)), \end{aligned} \quad (1.8)$$

where the longitudinal part of the polarization operator  $\hat{\mathbf{P}}_2^{\parallel}$  is replaced with the expectation (or c-number) value  $-\varepsilon_0 \tilde{\mathbf{E}}_2^{\parallel}$ .  $\tilde{\mathbf{E}}$  represents the near-field part of  $\mathbf{E}$ . Although the far-field part of  $\mathbf{E}$  can also be included in this derivation, we only use the near-field part for simplicity. Equation (1.8) is rewritten in a more compact form of

$$\begin{aligned} \hat{H}_{\text{mol}} - \int d\mathbf{r} \hat{\mathbf{P}}_1(\mathbf{r}) \cdot \tilde{\mathbf{E}}_2(\mathbf{r}, t) \\ - \int d\mathbf{r} [\hat{\mathbf{P}}_1(\mathbf{r}) \cdot \tilde{\mathbf{E}}_1^{\perp}(\mathbf{r}, t) + \hat{\mathbf{P}}_2(\mathbf{r}) \cdot (\tilde{\mathbf{E}}_1^{\perp}(\mathbf{r}, t) + \tilde{\mathbf{E}}_2^{\perp}(\mathbf{r}, t))], \end{aligned} \quad (1.9)$$

where we used the relations of  $\hat{\mathbf{P}}_1^{\parallel} \cdot \tilde{\mathbf{E}}_2^{\parallel} = \hat{\mathbf{P}}_1 \cdot \tilde{\mathbf{E}}_2^{\parallel}$  and  $\tilde{\mathbf{E}}_2^{\parallel} + \tilde{\mathbf{E}}_2^{\perp} = \tilde{\mathbf{E}}_2$ . Since the self-interaction term  $\hat{\mathbf{P}}_1 \cdot \tilde{\mathbf{E}}_1^{\perp}$  is not important in this work and  $\hat{\mathbf{P}}_2 \cdot (\tilde{\mathbf{E}}_1^{\perp} + \tilde{\mathbf{E}}_2^{\perp})$  does not act on the molecule 1, these terms can be omitted. Finally, the Hamiltonian of a molecule interacting with the near-field becomes

$$\hat{H} \equiv \hat{H}_{\text{mol}} + \hat{H}_{\text{int}}(t) = \hat{H}_{\text{mol}} - \int d\mathbf{r} \hat{\mathbf{P}}_1(\mathbf{r}) \cdot \tilde{\mathbf{E}}_2(\mathbf{r}, t). \quad (1.10)$$

This nonuniform light-matter interaction Hamiltonian is used throughout this study. Our computational model is rather oversimplified. However, it is computationally demanding to fully solved coupled Schrödinger–Maxwell equations, taking account of the properties of the self-consistency and the nonuniformity due to the light-matter interaction at the 1 nm scale. This derivation can also be applied to three or more particle systems, where only the dynamics of the molecule 1 interacting with the near-fields generated by the molecules 2, 3, ... is solved quantum mechanically in a similar way as in the two-particle system.

### 1.2.3 Near-Field Radiated from an Oscillating Dipole

Let us next model the near-field. The near-field is known to be a localized, non-propagating part of the light generated from a molecule when irradiated by an incident laser field (see Fig. 1.1). We describe the near-field in this article as the near-part of the electric field generated from an oscillating dipole, the simplest model for a radiation. In Fig. 1.3, the electric lines of the dipole radiation are depicted as the blue curves, the directions of which are shown by the arrows on the lines.



The analytical expression of the dipole radiation field  $\mathbf{E}_{\text{dip}}(\mathbf{r}, t)$  generated by the oscillating dipole is given by [36]

$$\mathbf{E}_{\text{dip}}(\mathbf{r}, t) = \frac{k^3}{4\pi\epsilon_0} \left( \frac{[3\mathbf{n}(\mathbf{n} \cdot \boldsymbol{\mu}) - \boldsymbol{\mu}]}{(kr)^3} \right. \quad (1.11a)$$

$$\left. - i \frac{[3\mathbf{n}(\mathbf{n} \cdot \dot{\boldsymbol{\mu}}) - \dot{\boldsymbol{\mu}}]}{(kr)^2} \right. \quad (1.11b)$$

$$\left. + \frac{[\mathbf{n} \times \dot{\boldsymbol{\mu}}] \times \mathbf{n}}{(kr)} \right) e^{-i\omega t + ikr} \quad (1.11c)$$

where  $k$  is a wavenumber,  $\epsilon_0$  is the vacuum permittivity,  $\mathbf{n}$  is the unit vector of  $\mathbf{r}/r$ ,  $\boldsymbol{\mu}$  is a dipole moment of the source placed at the origin, and  $\omega$  is a frequency of the oscillation, where  $\omega = kc$  with  $c$  being the velocity of light. The radiation field is classified into three parts in terms of the radial dependencies,  $r^{-3}$ ,  $r^{-2}$ , and  $r^{-1}$ . We set the distance between the target molecule and the radiation source to be several angstroms, which is comparable in size with the molecule. In this region, the dipole radiation field is dominated by the local electric field depending on  $r^{-3}$  given by Eq. (1.11a). This local field is referred to as the near-field  $\tilde{\mathbf{E}}$  used in the nonuniform light-matter interaction in Eq. (1.10). We can then neglect the magnetic interacting terms because the magnetic field from the oscillating dipole, not shown here, has the  $r^{-2}$  and  $r^{-1}$  dependent terms.

Since we consider an optical interaction between very closely spaced particles, it is reasonable to use the dipole radiation field as the electric near-field  $\tilde{\mathbf{E}}_2$  without distinguishing its longitudinal and transverse components. For larger systems, however, the longitudinal and transverse parts should be evaluated separately because there is a difference in time between them, i.e., the longitudinal interaction is instantaneous, whereas the transverse one is retarded. The retardation effect can be treated by solving the Maxwell equations using the time-dependent polarization as a radiation source.

### 1.2.4 Light-Matter Interaction in the Kohn-Sham DFT Approach

For computational applications of the present formal theory, we will derive the light-matter interaction  $H_{\text{int}}$  in the Kohn-Sham (KS) DFT form. In the following derivations, we take  $e_\alpha = -1$  for simplicity. Although the KS Hamiltonian is obtained by functional derivative of the expectation value of the total energy, it is enough to consider here only the light-matter interaction term of Eq. (1.10). The expectation value of  $\hat{H}_{\text{int}}$  is expressed by

$$\begin{aligned} \langle \hat{H}_{\text{int}}(t) \rangle &= \int d\mathbf{r} \Psi^*(\mathbf{r}, t) \hat{H}_{\text{int}}(t) \Psi(\mathbf{r}, t) \\ &= - \int d\mathbf{r} d\mathbf{r}' \Psi^*(\mathbf{r}, t) \hat{\mathbf{P}}(\mathbf{r}') \Psi(\mathbf{r}, t) \cdot \tilde{\mathbf{E}}(\mathbf{r}', t) \end{aligned}$$

$$\begin{aligned}
&= \int d\mathbf{r} d\mathbf{r}' \Psi^*(\mathbf{r}, t)(\mathbf{r} - \mathbf{R}) \\
&\quad \times \int_0^1 d\lambda \delta(\mathbf{r}' - \mathbf{R} - \lambda(\mathbf{r} - \mathbf{R})) \Psi(\mathbf{r}, t) \cdot \tilde{\mathbf{E}}(\mathbf{r}', t) \\
&= \int d\mathbf{r} [\Psi^*(\mathbf{r}, t) \Psi(\mathbf{r}, t)] (\mathbf{r} - \mathbf{R}) \int_0^1 d\lambda \\
&\quad \times \int d\mathbf{r}' \delta(\mathbf{r}' - \mathbf{R} - \lambda(\mathbf{r} - \mathbf{R})) \tilde{\mathbf{E}}(\mathbf{r}', t) \\
&\equiv \int d\mathbf{r} \rho(\mathbf{r}, t) (\mathbf{r} - \mathbf{R}) \cdot \int_0^1 d\lambda \tilde{\mathbf{E}}(\mathbf{R} + \lambda(\mathbf{r} - \mathbf{R}), t) \\
&\equiv \int d\mathbf{r} \rho(\mathbf{r}, t) (\mathbf{r} - \mathbf{R}) \cdot \mathbf{E}_{\text{eff}}(\mathbf{r}, t) \\
&\equiv \int d\mathbf{r} \rho(\mathbf{r}, t) V_{\text{eff}}(\mathbf{r}, t) \tag{1.12}
\end{aligned}$$

where  $\Psi$  is the ground state wavefunction of the molecule, and the electron density  $\rho(\mathbf{r})$ , the effective electric field  $\mathbf{E}_{\text{eff}}$ , and the effective potential  $V_{\text{eff}}$  are given by

$$\rho(\mathbf{r}, t) \equiv \Psi^*(\mathbf{r}, t) \Psi(\mathbf{r}, t), \tag{1.13a}$$

$$\mathbf{E}_{\text{eff}}(\mathbf{r}, t) \equiv \int_0^1 d\lambda \tilde{\mathbf{E}}(\mathbf{R} + \lambda(\mathbf{r} - \mathbf{R}), t), \tag{1.13b}$$

$$V_{\text{eff}}(\mathbf{r}, t) \equiv (\mathbf{r} - \mathbf{R}) \cdot \mathbf{E}_{\text{eff}}(\mathbf{r}, t). \tag{1.13c}$$

The  $\lambda$ -integration of  $\tilde{\mathbf{E}}$  includes all the contributions of the spatial variation of the electric field. As is clearly seen from Eq. (1.12), the nonuniform light-matter interaction is straightforwardly calculated in the conventional KS-DFT approach if the effective potential  $V_{\text{eff}}$  is added to the external potential term in the KS equation.

## 1.3 Computational Application

### 1.3.1 Time-Dependent Kohn-Sham Approach in Real Space

In this section, the KS-DFT computational approach is explained to demonstrate the electron dynamics of nanoclusters interacting with a near-field. The time-dependent Kohn-Sham (TD-KS) approach in real space and time to electron dynamics has so far been explained elsewhere [32, 37–39]. We review the approach with particular emphasis on extending it to the optical response to a nonuniform electric field. A time-dependent  $N$ -electron interacting system is solved through a set of electronic

wave functions  $\psi_j(\mathbf{r}, t)$  satisfying the following TD-KS equation

$$i\hbar \frac{\partial}{\partial t} \psi_j(\mathbf{r}, t) = \left[ -\frac{\hbar^2}{2m} \nabla^2 + V_{\text{KS}}[\rho](\mathbf{r}, t) \right] \psi_j(\mathbf{r}, t), \quad (1.14)$$

where  $m$  is the electron mass and  $\rho$  is the electron density given by

$$\rho(\mathbf{r}, t) = 2 \sum_{j=1}^{N/2} |\psi_j(\mathbf{r}, t)|^2. \quad (1.15)$$

The factor of 2 indicates that each KS orbital is fully occupied (i.e., a closed shell system). The KS potential  $V_{\text{KS}}[\rho](\mathbf{r}, t)$  is a functional of  $\rho$ , and it consists of four terms of an ion-electron interaction potential  $V_{\text{ion}}(\mathbf{r})$ , a time-dependent Hartree potential, an exchange-correlation (XC) potential  $V_{\text{xc}}[\rho](\mathbf{r}, t)$ , and an external potential  $V_{\text{eff}}$  as follows:

$$V_{\text{KS}}[\rho](\mathbf{r}, t) = V_{\text{ion}}(\mathbf{r}) + \frac{1}{4\pi\epsilon_0} \int \frac{\rho(\mathbf{r}', t)}{|\mathbf{r} - \mathbf{r}'|} d\mathbf{r}' + V_{\text{xc}}[\rho](\mathbf{r}, t) + V_{\text{eff}}(\mathbf{r}, t). \quad (1.16)$$

The ion-electron interaction potential  $V_{\text{ion}}(\mathbf{r})$  is constructed from norm-conserving pseudopotentials of each atomic component of the system considered. Following the Troullier and Martins procedure [40], the pseudopotentials are numerically generated so that the pseudowavefunctions can imitate the all-electron atomic wave functions. The potentials depend on the angular momentum components. In this article, we use the Kleinman-Bylander separable form to represent the nonlocal (i.e., angular momentum depending) potential terms [41].

To represent the XC potential, we use the following adiabatic local density approximation (ALDA)

$$V_{\text{xc}}[\rho](\mathbf{r}, t) \approx V_{\text{xc}}^{\text{LDA}}[\rho](\mathbf{r}, t) = V_{\text{xc}}^{\text{LDA}}[\rho_0](\mathbf{r})|_{\rho_0(\mathbf{r})=\rho(\mathbf{r}, t)}, \quad (1.17)$$

where  $V_{\text{xc}}^{\text{LDA}}[\rho_0](\mathbf{r})$  is the ground-state LDA XC potential given by Perdew and Zunger [42]. In ALDA, the XC potential at  $\mathbf{r}$  and  $t$  is approximated by that of the ground-state uniform electron gas having the density  $\rho(\mathbf{r}, t)$ . Although the ALDA XC potential does not take account of the nonlocality in both  $\mathbf{r}$  and  $t$  and more accurate exchange-correlation functionals have been developed lately, the ALDA has practically provided results for single-electron excitation processes sufficiently below the lowest ionization threshold of systems [43–45]. Furthermore, it is reasonable to use such a simple functional at this early stage of development prior to performing highly accurate calculations towards material science.

In the present theoretical model of the nonuniform light-matter interaction, the external potential  $V_{\text{eff}}$  is given by Eqs. (1.13b) and (1.13c). As mentioned above,  $\tilde{\mathbf{E}}$  in Eq. (1.13b) is approximated as the oscillating dipole radiation Eqs. (1.11a)–(1.11c), the main contribution of which is given by the  $r^{-3}$  dependent term of Eq. (1.11a). We set the center of mass of the molecule to be the origin. The temporal

shape of the near-field is taken as a pulse. Finally, the effective potential Eq. (1.13c) is rewritten by

$$V_{\text{eff}}(\mathbf{r}, t) = -\mathbf{r} \cdot \mathbf{E}_{\text{eff}}(\mathbf{r}) \sin(\omega t) \sin^2\left(\frac{\pi t}{T}\right) \quad (0 < t < T), \quad (1.18)$$

where  $\omega$  is the frequency of the oscillating dipole, and  $T$  determines the pulse duration. The pulse profile is approximated by  $\sin^2(\frac{\pi t}{T})$  in which a few cycles of the electric fields are included. The field intensity is related to the field strength by  $I = \frac{1}{2}\epsilon_0 c E^2$ .

## 1.4 High-Harmonic-Generation Spectra Induced by the Near-Field Excitation

### 1.4.1 Molecular System and Computations

A linear chain molecule is one of the better choices to demonstrate the nonuniform light-matter interaction, in particular for such an electric field proportional to  $r^{-3}$ . We choose a dicyanodiacetylene ( $\text{NC}_6\text{N}$ ) molecule [46] shown in Fig. 1.4(a) as an example of a real molecule. The geometric structure has been optimized by using the TURBOMOLE V5.10 [47, 48] package of quantum chemistry programs, employing the LDA exchange functional developed by Perdew and Wang [49] with the basis set of def-SV(P) [50] from the TURBOMOLE basis set library, which corresponds to the basis set of 6-31G\*. The simplest functional LDA was chosen for consistency with the functional used in the TD-KS equation. The vibrational analysis showed no imaginary frequency. The interatomic distances of the molecule are  $\text{N}_1\text{--C}_2 = 1.176 \text{ \AA}$ ,  $\text{C}_2\text{--C}_3 = 1.354 \text{ \AA}$ ,  $\text{C}_3\text{--C}_4 = 1.239 \text{ \AA}$ , and  $\text{C}_4\text{--C}_5 = 1.340 \text{ \AA}$ .<sup>1</sup>

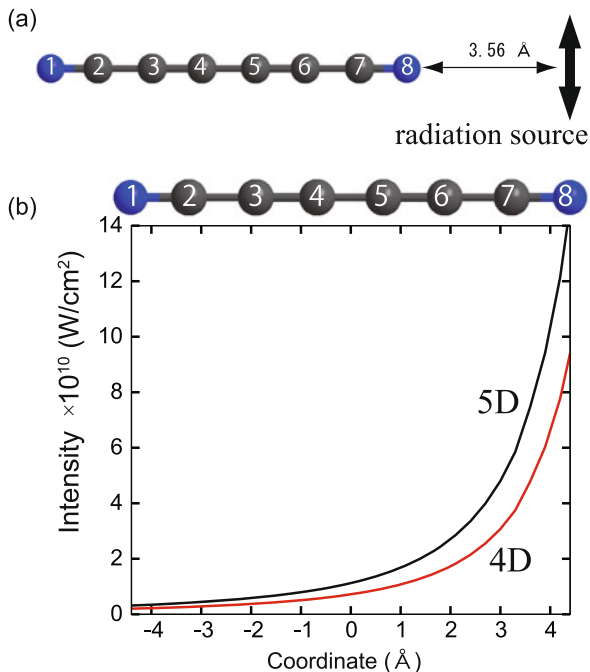
The TDKS equation (1.14) for  $\text{NC}_6\text{N}$  is solved numerically by a grid-based method [32, 51] in a three-dimensional Cartesian-coordinate rectangular box, the lengths of which are  $30 \text{ \AA}$  along the molecular ( $x$ -) axis and  $20 \text{ \AA}$  along the  $y$ - and  $z$ -axes, utilizing uniform grids with a mesh spacing of  $0.3 \text{ \AA}$ . The Laplacian operator is evaluated by a nine-point difference formula [52]. The time-propagation of the KS orbitals is carried out with a fourth-order Taylor expansion by using a constant time step of  $0.002 \text{ fs}$ . The inner shell structures of the carbon and nitrogen atoms are approximated by effective core pseudopotentials, and then the remaining four electrons ( $2s^2 2p^2$ ) for C and five electrons ( $2s^2 2p^3$ ) for N are explicitly treated. In other words, we have carried out 34-electron dynamics calculations for  $\text{NC}_6\text{N}$ .

The effective potential for the dipole radiation on each grid is computed combining Eqs. (1.11a)–(1.11c), (1.13b), and (1.13c), where the main contribution in Eqs. (1.11a)–(1.11c) is its near-field part (1.11a). A point dipole  $\boldsymbol{\mu}$  is placed at

---

<sup>1</sup>These bond lengths remain almost unchanged (i.e., at most  $0.0024 \text{ \AA}$  for  $\text{C}_3\text{--C}_4$ ) even if the geometry optimization was performed by using the B3LYP functional [58, 59].

**Fig. 1.4** (a) Geometrical structure of NC<sub>6</sub>N and the position of the radiation source. (b) The intensities of the effective electric fields on the molecular axis calculated from the near-field of the dipole radiation. The near-fields are generated by the oscillating dipole with its absolute value of the dipole moment being 4 D and 5 D, respectively

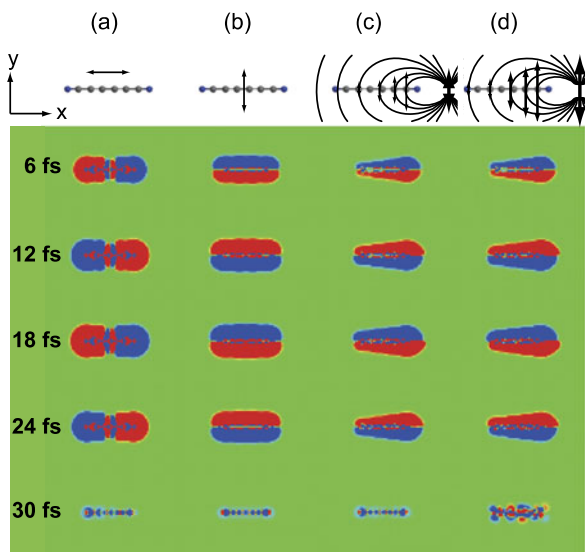


$x = 8.0$  Å (i.e., the value of  $3.56$  Å is the distance between the rightmost nitrogen atom N(8) and the dipole as shown in Fig. 1.4(a)) so that the nonuniform electronic excitation due to the near-field is clearly demonstrated. The dipole is assumed to be  $y$ -polarized, that is  $\boldsymbol{\mu} = (0.0, \mu, 0.0)$  Debye (D), where  $\mu$  is the absolute value of the dipole moment. The dipole fields generated from  $\mu = 4.0$  D and  $5.0$  D are used in this study. The integral of Eq. (1.13b) is calculated numerically with a constant step of  $\Delta\lambda = 0.0423$  Å. The contribution of the dipole radiation field at its origin to the integration is evaluated by  $4\pi\boldsymbol{\mu}/3$  [31].  $E_{\text{dip}}$  is also replaced with  $4\pi\boldsymbol{\mu}/3$  if  $|E_{\text{dip}}|$  is larger than  $|4\pi\boldsymbol{\mu}/3|$ . This is done for a few points very close to the dipole, i.e.,  $|r| \sim 0.2$  Å. The intensity of the effective electric field varies largely as indicated in Fig. 1.4(b). The effective field intensity at the right end of the NC<sub>6</sub>N molecule is two orders of magnitude larger than that at the left end (i.e.,  $10^{11}$  and  $10^9$  W/cm<sup>2</sup> at the right and the left ends, respectively). Thus, the molecule is nonuniformly excited by the oscillating dipole field. All the electric fields used in this study have the field frequency  $\omega$  of 1 eV (the off-resonance condition). The pulse duration ( $T = 30$  fs) is short enough to avoid considering the nuclear dynamics.

### 1.4.2 Near-Field Excitation Dynamics

Let us first demonstrate the electron density motions in the uniform and the nonuniform electric fields. Figure 1.5 shows four snapshots of differences of the electron

**Fig. 1.5** Snapshots of difference of the electron density at  $t = 6, 12, 18, 24$ , and 30 fs from the initial ( $t = 0$  fs) static electron density. The uniform fields ((a), (b)) and the nonuniform (oscillating dipole) fields with their dipole moments being (c) 4 D and (d) 5 D are applied to the molecule. Four schematic illustrations at the top of each snapshot display the ways of electronic excitation



densities at  $t = 6, 12, 18, 24$ , and 30 fs from the initial ( $t = 0$ ) electron density. Each snapshot indicates an increase and a decrease in the electron density, respectively. Each column of the snapshots illustrates the different time evolution of the electron density depending on the ways of electronic excitation. Four schematic illustrations at the top of the figure display how the light-matter interaction works. The uniform oscillating-electric-field with its intensity of  $10^{12}$  W/cm<sup>2</sup> is applied to the molecule along the (a)  $x$ - or (b)  $y$ -axis, whereas the nonuniform fields radiated from the oscillating dipoles (the black bold arrows) with their dipole moments being (c) 4 D and (d) 5 D are applied to the molecule.

The electron densities in Figs. 1.5(a) and (b) oscillate uniformly and regularly along the applied field directions, keeping the molecular symmetry. However, as shown in Figs. 1.5(c) and (d), the nonuniform electric field apparently induces the symmetry-breaking time-evolution of the electron density. Such inhomogeneous electron dynamics clearly reflects the spatial distribution of the dipole field. Since the oscillating dipole is  $y$ -polarized, the generated electric field on the  $x$ -axis is also  $y$ -polarized, but its intensity sharply falls as  $r$  increases (i.e.,  $\propto r^{-3}$ ), where  $r$  is the distance from the oscillating dipole. Furthermore, only the  $x$ -component of the dipole field  $E_x$  is antisymmetric with respect to the  $x$ -axis (i.e.,  $E_x(x, y, z) = -E_x(x, -y, z)$ ), whereas  $E_y$  and  $E_z$  are symmetric. For these reasons, the time-evolved densities in Figs. 1.5(c) and (d) regularly oscillate to some extent along the  $y$ -axis, whereas those are distorted along the  $x$ -axis. The electron density distributions at 12 and 18 fs, for example, represent the antisymmetric motion along the  $x$ -axis. Specifically, the upper and lower half parts of the densities with respect to the  $x$ -axis move toward the opposite directions. These irregular motions are really due to the electronic excitation by the symmetry-breaking, nonuniform electric field. The electron density distribution at 30 fs in Fig. 1.5(d) looks

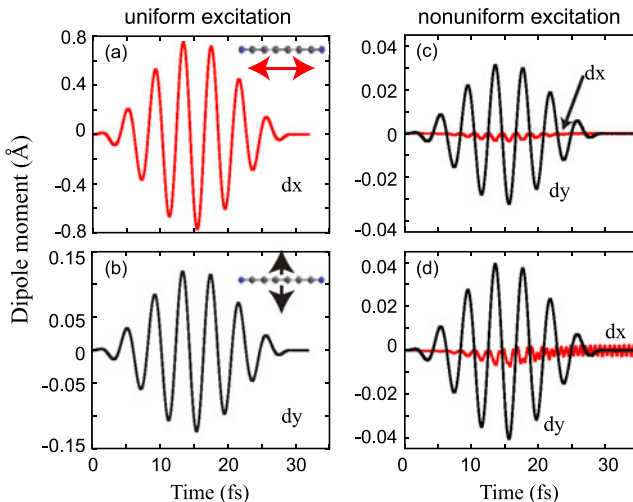
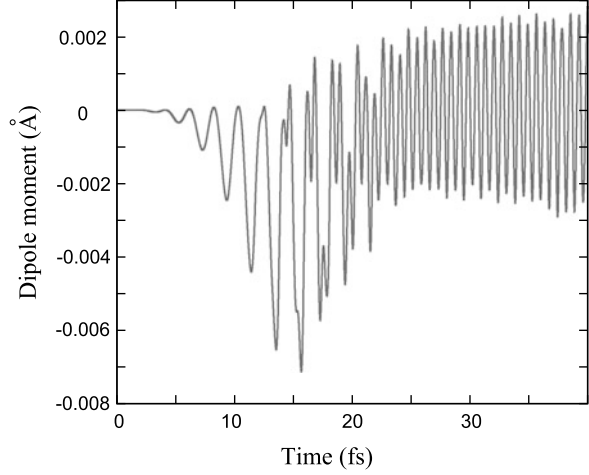


**Fig. 1.6** Induced dipole moments along the  $x$ - and  $y$ -axes,  $d_i$  ( $i = x, y$ ). The dipole moments, respectively, correspond to the time-evolutions of the density in Figs. 1.5(a)–(d). Insets in (a) and (b) are schemes of the applied field direction

rather different from the others. The electron-density-differences in Figs. 1.5(a)–(c) almost disappear at the end of the pulse of the external electric fields because the applied laser frequency considered is not in tune with any resonance frequencies. In contrast, the electron density distribution in Fig. 1.5(d), under the condition of the stronger nonuniform electric field, still persists even after the end of the pulsed near-field. This is attributed to the nonuniform excitation by the localized near-field. In this study, the near-field frequency is not tune with any dipole resonance frequencies of NC<sub>6</sub>N. Thus, the time-evolution of the electron density should not persist after the end of the near-field radiation (see, Fig. 1.5(c)). However, higher harmonics are more easily generated by the nonuniform excitation with increasing the strength of the dipole radiation field. NC<sub>6</sub>N has a dipole resonance frequency at 5.75 eV, which is close to the sixth harmonics (=6 eV). As the result of this, the resonance excitation accidentally occurs in the case of Fig. 1.5(d). Such a resonance excitation allows the electrons to move persistently after the end of the pulse. It should be noted that this resonance effect is due to a high-order nonlinear effect and thus is still minor in the present nonuniform light-matter interaction model, i.e., it hardly affects the radiation from the molecule 2.

Figures 1.6(a)–(d) show the induced dipole moments along the  $x$ - and  $y$ -axes,  $d_i$  ( $i = x, y$ ), corresponding to the time evolutions of the electron densities in Figs. 1.5(a)–(d), respectively. The red and the dashed black curves represent  $d_x$  and  $d_y$ . The insets in Figs. 1.6(a) and (b) schematically draw the applied field directions. Similar overall time-profiles have been observed in  $d_x$  (Fig. 1.6(a)) and  $d_y$  (Fig. 1.6(b)) induced by the uniform field and in  $d_y$  induced by the nonuniform field. In sharp contrast, nonuniformly induced  $d_x$ s do not follow the time-profile of the applied field. To see this more clearly, we pick up  $d_x$  in Fig. 1.6(d) and plot it

**Fig. 1.7** Magnification of  $d_x$  in Fig. 1.6(d)



in Fig. 1.7. In the early times until about 20 fs,  $d_x$  takes negative values owing to the sharp gradient in the field intensity. The oscillation frequency becomes much faster than that of the applied field after  $\sim 20$  fs. Such an irregular oscillation of  $d_x$  is a consequence of the antisymmetric  $E_x$  of the dipole field that acts strongly in the right part of NC<sub>6</sub>N. Thus, the irregular time-evolutions of the density along the  $x$ -axis in Figs. 1.5(c) and (d) were induced by the nonuniform, antisymmetric dipole radiation field. We have further confirmed that such an irregular motion cannot be induced even if we use either an electric field having a similar sharp gradient in the field intensity or an antisymmetric electric field.

We next calculate the emission spectra for each electron dynamics to analyze the uniform and nonuniform electronic excitations in an energy domain. Since the emission spectrum is associated with the dipole acceleration [53, 54], we here take the second derivative of the induced dipole moments and then perform a Fourier transform. Figure 1.8 shows the power spectra of the dipole acceleration  $|\ddot{d}_i(\omega)|^2$  ( $i = x, y$ ) in the unit of  $\text{\AA}^2 \text{fs}^{-2}$  as a function of energy. We refer to the power spectra of the dipole acceleration as harmonic-generation (HG) spectra. The HG spectra in Figs. 1.8(a)–(d) correspond to the induced dipole moments in Figs. 1.6(a)–(d), respectively. The red and the dashed black curves represent  $|\ddot{d}_x(\omega)|^2$  and  $|\ddot{d}_y(\omega)|^2$ . Comparing Figs. 1.8(a) and (b), the harmonics along the  $x$ -axis ( $\ddot{d}_x$ ) seem relatively easier to generate than that along the  $y$ -axis ( $\ddot{d}_y$ ). A comparatively large peak appears at around 6 eV in Fig. 1.8(a). As discussed in the time-evolution of the electron density in Fig. 1.5, this large peak is due to the fact that the sixth harmonics is accidentally close to a dipole resonance peak ( $=5.75$  eV) of NC<sub>6</sub>N. Despite the inversion symmetry of NC<sub>6</sub>N, the nonuniform electric field, in contrast to the uniform one, causes the even harmonics in addition to the odd harmonics as shown in Figs. 1.8(c) and (d). Interestingly, the even and odd harmonics are respectively due to the induced dipole moments along the  $x$ - and  $y$ -axes. The even harmonics, therefore, have proved to be generated by the nonuniform electric field breaking the symmetry along the  $x$ -axis. Furthermore, in comparison with the



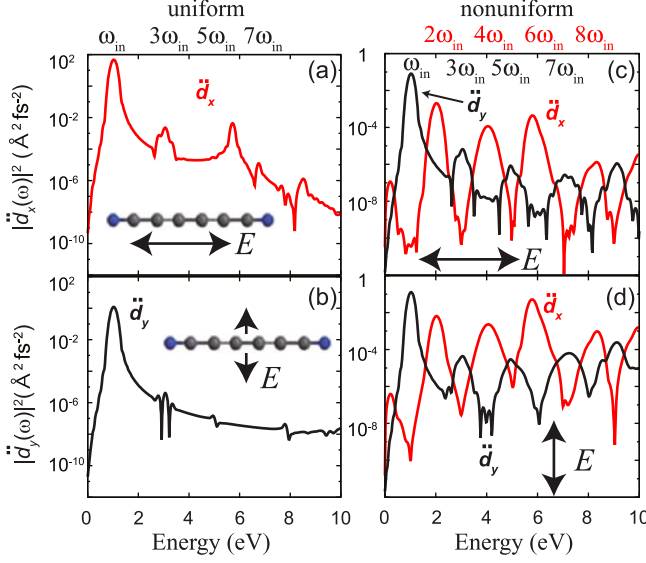


**Fig. 1.8** HG power spectra of the dipole acceleration. The ways of electronic excitation correspond to those in Figs. 1.5(a)–(d) and also in Figs. 1.6(a)–(d), respectively

HG spectra by the uniform electric field, relatively higher harmonics are clearly seen in the HG spectra by the nonuniform electric field. In addition, their peak intensities do not decay linearly against the order of the harmonics.

Before ending this section, we demonstrate that the nonuniform electronic excitation also induces the quadrupole moment, which is never induced by the uniform electric field, as one of the phenomena beyond the dipole approximation. Such non-dipole excitation was observed in an experiment [55], although both nanostructure systems are different from the present one. The  $xy$  component of the quadrupole moment ( $Q_{xy}$ ) for the time-evolution of Fig. 1.5(d) and its HG power spectrum are shown in Figs. 1.9(a) and (b), respectively. The quadrupole moments both in the time and the energy domains provide the structural patterns quite similar to those of the dipole ones. To verify that  $Q_{xy}$  is non-negligible in the nonuniform excitation, we consider the charge distribution that causes dipole and quadrupole moments. The calculated value of the quadrupole moment in the unit of  $\text{\AA}^2$  is about an order of magnitude larger than that of the dipole moment in the unit of  $\text{\AA}$ . The dipole moment of two charges  $q$  and  $-q$  with the inter charge distance  $a$  is  $qa \text{ \AA}$ , whereas the quadrupole moment of two positive  $q'$  and two negative  $-q'$  charges disposed at the corners of a square with its side being  $a$  is  $q'a^2 \text{ \AA}^2$ . Then,  $|Q_{xy}| \sim 10|d_y|$  (see Figs. 1.6(d) and 1.9(a)) and  $a$  is  $\sim 10 \text{ \AA}$  for NC<sub>6</sub>N. Thus, we have  $q \sim q'$  because  $q'a^2 \sim 10 \times qa \rightarrow q'a \sim 10 \times q \rightarrow q' \sim q$ . This indicates that the dipole-like and quadrupole-like charge distributions have been induced in almost the same amount as a consequence of the nonuniform light-matter interaction.

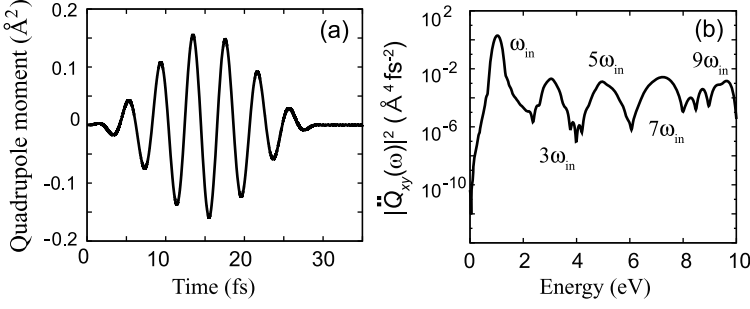


**Fig. 1.9** (a)  $xy$ -component of the induced quadrupole moment as a result of the nonuniform excitation with  $\mu = 5$  D and (b) its power spectrum

### 1.4.3 Even and Odd Harmonics

Let us next carry out a perturbation analysis of the HG power spectra generated through the nonuniform light-matter interaction. As shown in Figs. 1.8(c) and (d), the even harmonics appear despite the inversion symmetry of NC<sub>6</sub>N. The even and odd harmonics are due to the induced dipole moments  $d_x$  and  $d_y$ , respectively. This even and odd alteration is easily understood in terms of the symmetries of the molecular wave functions and the external field.

According to the time-dependent perturbation theory [56, 57],  $n$ -th dipole moment  $d_\alpha^{(n)}$  ( $n = 1, 2, \dots$  and  $\alpha = x, y, z$ ) in powers of the perturbation  $V_{\text{eff}}$  can be evaluated by the following matrix elements,

$$\langle 0 | \alpha | i \rangle \underbrace{\langle i | V_{\text{eff}} | j \rangle \langle j | V_{\text{eff}} | k \rangle \cdots \langle l | V_{\text{eff}} | 0 \rangle}_{n \text{ brackets}}, \quad (1.19)$$

where  $|0\rangle$  and  $|i\rangle$  are the ground and the excited eigen states of the nonperturbative Hamiltonian of the molecule, respectively. As typical examples,  $d_x^{(2)}$ ,  $d_y^{(2)}$ ,  $d_x^{(3)}$ , and  $d_y^{(3)}$  are considered. Table 1.1 summarizes the evaluation of the matrix elements of  $d_x^{(2)}$  and  $d_y^{(2)}$ . The symmetries of the eigen states and the applied field are labeled as “*e*” for the even symmetry and “*o*” for the odd one. Since NC<sub>6</sub>N has mirror symmetries in every direction, the eigen state  $\{|i\rangle\}$  is either even or odd with respect to  $x$ -,  $y$ -, or  $z$ -axis, namely,  $\psi(x, y, z) = \pm\psi(-x, y, z)$ ,  $\psi(x, y, z) = \pm\psi(x, -y, z)$ , or  $\psi(x, y, z) = \pm\psi(x, y, -z)$ . The effective potential  $V_{\text{eff}}$  given by Eq. (1.13c) is neither an even nor an odd function of  $x$ , an odd function of  $y$ , and an even function of  $z$ , i.e.,  $V_{\text{eff}}(x, y, z) \neq V_{\text{eff}}(-x, y, z)$ ,  $V_{\text{eff}}(x, y, z) = -V_{\text{eff}}(x, -y, z)$ , and  $V_{\text{eff}}(x, y, z) = V_{\text{eff}}(x, y, -z)$ . Thus, the brackets can be estimated by decomposing them into the integrations with respect to the  $x$ -,  $y$ -, and  $z$ -coordinates.  $\int d\alpha$  ( $\alpha = x, y, z$ ) in Table 1.1 denotes each component of the integrations. The symmetries of the ground state  $|0\rangle$ , the operators ( $x$  and  $y$ ), and the potential  $V_{\text{eff}}$  are specified in bold characters. The symmetries of  $|i\rangle$  and  $|j\rangle$  are then specified so that the matrix elements have nonzero values. As a result,  $d_x^{(2)}$  becomes nonzero, but

**Table 1.1** Matrix elements of the second-order dipole moments along the  $x$ - and  $y$ -axes in the power of  $V_{\text{eff}}$ .  $e$  and  $o$  denote even and odd symmetries, respectively. The symmetries of the ground state and  $V_{\text{eff}}$  are indicated by bold characters

$d_x^{(2)}$	$\langle 0 x i \rangle$	$\langle i V_{\text{eff}} j \rangle$	$\langle j V_{\text{eff}} 0 \rangle$	
$\int dx$	$\langle e o o \rangle$	$\langle o eo eo \rangle$	$\langle eo eo e \rangle$	$\neq 0$
$\int dy$	$\langle e  e \rangle$	$\langle e o o \rangle$	$\langle o o e \rangle$	$\neq 0$
$\int dz$	$\langle e  e \rangle$	$\langle e e e \rangle$	$\langle e e e \rangle$	$\neq 0$
$d_y^{(2)}$	$\langle 0 y i \rangle$	$\langle i V_{\text{eff}} j \rangle$	$\langle j V_{\text{eff}} 0 \rangle$	
$\int dx$	$\langle e  e \rangle$	$\langle e eo eo \rangle$	$\langle eo eo e \rangle$	$\neq 0$
$\int dy$	$\langle e o o \rangle$	$\langle o o e \rangle$	$\langle e o e \rangle$	$= 0$
$\int dz$	$\langle e  e \rangle$	$\langle e e e \rangle$	$\langle e e e \rangle$	$\neq 0$

**Table 1.2** Same as Table 1.1 but for the third-order dipole moments. As in the case of Table 1.1,  $\int dx dz$  is always nonzero, and thus only  $\int dy$  is summarized here

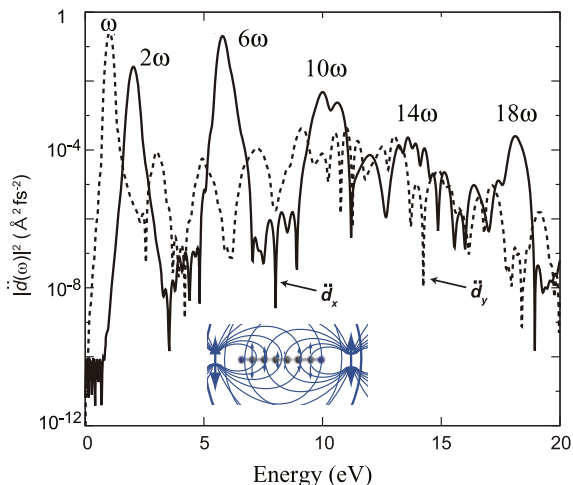
$d_x^{(3)}$	$\langle 0 x i \rangle$	$\langle i V_{\text{eff}} j \rangle$	$\langle j V_{\text{eff}} k \rangle$	$\langle k V_{\text{eff}} 0 \rangle$	
$\int dy$	$\langle e  e \rangle$	$\langle e o o \rangle$	$\langle o o e \rangle$	$\langle e o e \rangle$	$= 0$
$d_y^{(3)}$	$\langle 0 y i \rangle$	$\langle i V_{\text{eff}} j \rangle$	$\langle j V_{\text{eff}} k \rangle$	$\langle k V_{\text{eff}} 0 \rangle$	
$\int dy$	$\langle e o o \rangle$	$\langle o o e \rangle$	$\langle e o e \rangle$	$\langle o o e \rangle$	$\neq 0$

$d_y^{(2)}$  must be zero because the integral of  $\langle j|V_{\text{eff}}|0 \rangle$  with respect to the  $y$ -coordinate vanishes. The same analysis can be applied to  $d_x^{(3)}$  (see, Table 1.2). Then,  $d_x^{(3)}$  must be zero but  $d_y^{(3)}$  becomes nonzero. The above analysis clearly explains the even-odd alteration appears in the HG power spectra obtained by the nonuniform excitation.

#### 1.4.4 Control of Harmonic Generation by Interference

Finally, it is demonstrated that the harmonics induced by the near-field can be controlled. Figure 1.10 shows the HG power spectra obtained when both ends of the NC<sub>6</sub>N molecule are excited by the near-fields radiated from two oscillating dipoles with different phases by  $\pi/2$ . The inset illustrates the schematic diagram of the near-field excitation by two radiation sources. It is clearly seen from the figure that harmonics selectively appear every  $4\omega_{\text{in}}$  starting from the second harmonics ( $2\omega_{\text{in}}$ ). The fourth and eighth harmonics ( $4\omega_{\text{in}}$  and  $8\omega_{\text{in}}$ ) completely disappear as a result of the interference between the two near-fields having different phases. We expect that this idea of the near-field excitation with different phases can control intensities and orders of HG spectra.

**Fig. 1.10** Power spectra of the dipole acceleration along the  $x$ - and  $y$ -axes. Two oscillating dipole fields with different phases disposed at both ends of the molecule are applied



### 1.4.5 Concluding Remarks

We have presented a generalized theoretical description of optical response in an effort to understand a nonuniform light-matter interaction between a near-field and a 1-nm-sized molecule. The light-matter interaction based on the multipolar Hamiltonian, instead of the minimal coupling Hamiltonian, was described in terms of a space integral of the inner product of the total polarization of a molecule and an external electric field. Noteworthy is the fact that the polarization in the integral can be treated entirely without invoking any approximation such as a dipole approximation. Therefore, the present light-matter interaction theory allows us to understand the inhomogeneous electron dynamics associated with local electronic structures of a molecule at the 1 nm scale, although the wavelength of an incident laser pulse is much longer than the size of the molecule. For a computational application, we have studied the near-field-induced electron dynamics of NC<sub>6</sub>N by using the TD-KS approach in real space incorporated with the present nonuniform interaction theory. The electron dynamics induced by the nonuniform light-matter interaction is completely different from that by the conventional uniform interaction under the dipole approximation. Specifically, in the nonuniform electronic excitation high harmonics were generated more easily and much more interestingly the even harmonics were also generated in addition to the odd ones despite the inversion symmetry of NC<sub>6</sub>N. Perturbation theory clearly explained that the even harmonics were generated owing to the symmetry-breaking (nonuniform) electric field along the  $x$ -axis radiated from the oscillating dipole. It has also been found that the nonuniform fields with different phases control HG though their interference effect.

## 1.5 Near-Field Induced Optical Force in a Metal Nanoparticle and C<sub>60</sub>

### 1.5.1 Brief Review of Optical Force

Optical trapping of micron-sized particles by lasers was reported in the pioneering work by Ashkin [60] and its idea was eventually realized as an innovative tool of a single-beam gradient force optical trap for dielectric particles, called “optical tweezers” [61]. In a series of papers since this seminal work, Ashkin and coworkers have succeeded in optically trapping and manipulating various types of objects [62]. The optical tweezers using force exerted by a highly focused laser-beam can trap and manipulate objects, now in practice, ranging in force up to 100–200 pN with sub-pN resolution and in size from tens of nanometers to tens of micrometers. Such laser-based optical traps have been used in a wide-range of applications [63, 64] to atoms and small molecules [62], colloidal particles [65, 66], and biological objects [67–69]. In particular, biological applications have been extensively made to study mechanical or functional properties of cells, intercellular materials, and filaments, and also to study biological motors. A large number of references of those biological applications were compiled in the resource letters [70].

Although a complete description of the laser-based optical traps needs a fully quantum-mechanical treatment, the optical force exerted on trapped objects can be derived from the Maxwell stress tensor into two limiting cases where the size of the object is much larger (i.e., infinitely extended systems) and much smaller (i.e., small particle systems) than the wavelength of an incident laser field [6]. In the limiting case of the extended systems, the net force is associated with so called optical pressure. In the other limiting case of the small particle systems, the net force considered to be a gradient force. Since in this article we study nanoparticle and light interaction, the gradient force exerted by optical field is only discussed. The gradient force is expected to be exerted more efficiently by using a near-field in optical traps because the near-field is a very short-ranged electromagnetic field with strong intensity gradient. Such a short-ranged field has the advantage of improving resolution beyond the diffraction limit. In addition, the near-field enhancement, which is a consequence of self-consistent light-matter interaction, enables to trap objects with weaker intensity of an incident laser beam. Novotny and coworkers proposed a theoretical scheme for using optical forces by the near-field close to a laser-illuminated metal tip [71]. They demonstrated that strong mechanical force and torque were exerted on dielectric particles in aqueous environments at the nanometer scale.

In recent years, laser-based optical phenomena in nanostructures including optical traps mentioned above have been intensively studied in a rapidly growing research area, referred to as “nano-optics” or “nanophotonics”. The fundamental features of those optical phenomena are understood in the more general context of light-matter interaction in optical response theory. A semiclassical approach has so far been employed to understand these phenomena because a fully quantum mechanical treatment, i.e., quantum electrodynamics theory, is almost impossible in

practice to perform for real nanostructure systems. In the semiclassical approach, an optical field is determined by the Maxwell equation and a material is described quantum mechanically, and the resulting Maxwell and Schrödinger coupled equation should be solved self-consistently [21–23]. However, it is still computationally highly demanding to carry out the coupled equation in real systems [72, 73]. Instead of treating the coupled equation rigorously, many authors employed numerically feasible approaches in which, particularly, the target objects were phenomenologically approximated by model materials such as dielectrics to avoid fully solving electronic structure calculations [71, 74–78].

Detailed electronic structures of molecules play an essential role in molecular science because they determine all the properties of materials such as geometry, bonding character, stability, functionality, reactivity, and so forth. In general, absorption spectra of molecules become discrete with many sharp peaks as the system decreases in size. Each peak is apparently associated with detailed electronic structures consisting of discrete energy levels of molecules. This is due to the fact that the light-matter interaction in such molecular systems can change drastically depending on the electronic structures. One simple and clear example is resonance effect in absorption spectra. As easily inferred from this characteristic, the optical force also strongly depends on details of the electronic structures of nanometer-sized objects. This means that we can optically trap and manipulate an object more precisely by changing the incident laser frequency or the position of the exerted force on an object. For these reasons, it is very important to analyze the optical force on nanostructures, explicitly taking account of the electronic structures of objects.

As described in the previous section, we recently reported the first-principles electron dynamics simulation approach to solving optical response fully taking account of nonuniform light and matter interaction [79]. This approach has following advantages.

- (i) Electronic structure and electron dynamics calculations are carried out at the level of density functional theory (DFT) and time-dependent (TD) DFT, respectively.
- (ii) Full nonuniform-light and matter interactions (i.e., full-multipole effects) are included.
- (iii) Electron dynamics simulation in real space and real time makes it much easier to analyze and visualize optical response of a target molecule.

We here employ this approach to understand the mechanisms of the optical force exerted on nanostructures interacting with a near-field. Special emphasis is placed on elucidating the effect of the detailed molecular-electronic-structures on the optical force.

### ***1.5.2 Optical Force Exerted on a Particle***

Optical response to the near-field has been described in the previous section. Here, we present the method of calculations of optical force exerted on a particle. The

optical force exerted on the center of mass of a nanoparticle in the time-domain can be written in the form of

$$\mathbf{F}(t) = - \int [\rho(\mathbf{r}, t) - \rho(\mathbf{r}, 0)] \mathbf{E}(\mathbf{r}, t) d\mathbf{r}. \quad (1.20)$$

It should be noted that  $\rho(\mathbf{r}, t) - \rho(\mathbf{r}, 0)$  is the net or true induced charge distribution and numerically includes the full contributions of the charges screening the external electric field within the molecule, i.e., an internal electric field effect. To obtain the net force, the time-average of this quantity over the pulse duration  $T$  is taken,

$$\langle \mathbf{F} \rangle = \frac{1}{T} \int_0^T \mathbf{F}(t) dt. \quad (1.21)$$

If a target material has a complex structure unlike a sphere used in this paper, it might be useful to define local optical forces acting on each local structure of a material.

We do not consider the damping effect due to an electron-nuclear coupling or thermal relaxation on the electron dynamics. Thus, the response of the molecule could be artificially strong in the present model. Ideally, it is necessary to treat the electron dynamics in the presence of such relaxation, although it is practically almost impossible in real nanostructure systems. In an effort to accurately describe optical force exerted on molecules at the level of molecular theory, we here carry out the first-principles calculations of electron dynamics as a first step and leave the relaxation effect for future investigation.

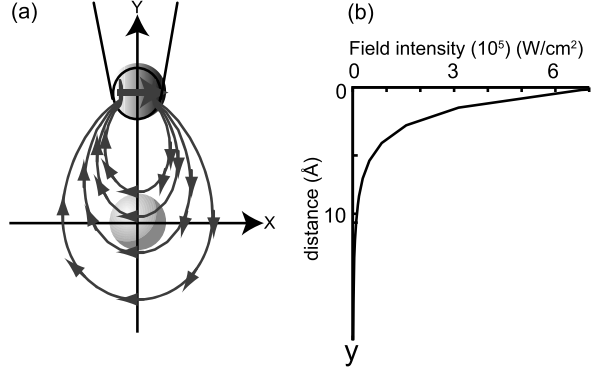
### 1.5.3 Model System and Computations

We consider that a nanoparticle interacts with the near-field radiated from an  $x$ -polarized oscillating dipole at 10 Å above the molecule center,  $(x, y, z) = (0, 0, 0)$ , as shown in Fig. 1.11(a). The spatial distribution of the near-field is given by [36]

$$\mathbf{E}(\mathbf{r} - \mathbf{R}_{\text{dip}}) = \frac{[3\mathbf{n}(\mathbf{n} \cdot \boldsymbol{\mu}) - \boldsymbol{\mu}]}{(4\pi\epsilon_0|\mathbf{r} - \mathbf{R}_{\text{dip}}|)^3} e^{ik \cdot (\mathbf{r} - \mathbf{R}_{\text{dip}})}, \quad (1.22)$$

where  $\mathbf{R}_{\text{dip}}$  is the coordinate of the oscillating dipole,  $k$  is the wavenumber,  $\epsilon_0$  is the vacuum permittivity,  $\mathbf{n}$  is the unit vector of  $(\mathbf{r} - \mathbf{R}_{\text{dip}})/|\mathbf{r} - \mathbf{R}_{\text{dip}}|$  and  $\boldsymbol{\mu}$  is the dipole moment of the radiation source. We set  $\mathbf{R}_{\text{dip}} = (0.0, 10.0, 0.0)$  Å and  $\boldsymbol{\mu} = (0.01, 0.0, 0.0)$  Debye. As shown in Fig. 1.11(b), the intensities of the near-field are  $7.4 \times 10^5$ ,  $1.2 \times 10^4$ , and  $1.0 \times 10^3$  W/cm<sup>2</sup> at  $(x, y) = (0.0, 5.0)$ ,  $(0.0, 0.0)$ , and  $(0.0, -5.0)$  Å, respectively. The external potential  $V_{\text{eff}}$  is calculated by Eq. (1.13c) with the effective electric field Eq. (1.13b) where the electric field  $\mathbf{E}$  is given by the dipole radiation, Eq. (1.22). We set the center of mass of the molecule to be the

**Fig. 1.11** (a) Schematic of a near-field fiber tip (*upper ball*) and a target particle (*lower ball*). The near-field is approximated by the radiation from an  $x$ -polarized oscillating dipole (*solid arrow*). The *thin curves with arrows* denote the electric field lines. (b) Electric field intensity as a function of distance between the tip and the particle



origin. The temporal shape of the near-field is taken as a pulse. Finally, the effective potential Eq. (1.13c) is rewritten by

$$V_{\text{eff}}(\mathbf{r}, t) = -\mathbf{r} \cdot \mathbf{E}_{\text{eff}}(\mathbf{r}) \sin(\omega t) \sin^2\left(\frac{\pi t}{T}\right) \quad (0 < t < T), \quad (1.23)$$

where  $\omega$  is the frequency of the oscillating dipole, and  $T$  determines the pulse duration.

We demonstrate the TDDFT simulation of the optical force in different two systems: a metal nanoparticle and  $\text{C}_{60}$ . The metal nanoparticle is simplified by a jellium model, in which the ionic background is given by

$$V_{\text{ion}}(\mathbf{r}) = \frac{3}{4\pi r_s^3} \left[ 1 + \exp\left(\frac{|\mathbf{r}| - a}{w}\right) \right]^{-1}, \quad (1.24)$$

where  $r_s$  is the density parameter [80],  $a$  is the radius of the sphere and  $w$  is the smoothed out factor for the jellium surface. The jellium parameters for the metal nanoparticle are set to  $r_s = 1.60$ , which corresponds to a silver atom (34 electrons),  $a = 0.5 \text{ nm}$ , and  $w = 0.538$ . For  $\text{C}_{60}$ , on the other hand, the ionic background  $V_{\text{ion}}(\mathbf{r})$  of an atomic component C is constructed from a norm-conserving pseudopotential generated numerically following the Troullier and Martins procedure [40]. In this article, we use the Kleinman-Bylander separable form to represent the nonlocal (i.e., angular momentum depending) potential terms [41]. The C–C distances are set to be  $1.457 \text{ Å}$  for the single bond and  $1.384 \text{ Å}$  for the double bond. The inner shell structure of the carbon atom is approximated by an effective core pseudopotential, and then the remaining four electrons ( $2s^2 2p^2$ ) are explicitly treated, i.e., 240-electron dynamics simulation in total for  $\text{C}_{60}$ . To represent the exchange-correlation potential  $V_{\text{xc}}(\mathbf{r}, t)$ , we use the local density approximation given by Perdew and Zunger [42] as in the previous study.

The computational approach is based on TDKS. The approach was described in the previous section. The TDKS equation (1.14) for these particles is solved numerically by a grid-based method [25, 32, 33, 35, 38, 39, 51, 52] in a three-dimensional Cartesian-coordinate cubic box. For the metal particle, the length of the cubic box is



26 Å and the uniform grids with a mesh spacing of 0.5 Å are used, while the length and the mesh spacing are 16 Å and 0.3 Å, respectively, for C<sub>60</sub>. The Laplacian operator is evaluated by a nine-point difference formula [52]. The time-propagation of the KS orbitals is carried out with a fourth-order Taylor expansion by using a constant time step of 0.005 fs for the metal particle and 0.002 fs for C<sub>60</sub>.

The effective potential for the dipole radiation on each grid is computed combining Eqs. (1.13b), (1.13c), and (1.22). The integral of Eq. (1.13b) is calculated numerically with a constant spacing of  $\Delta\lambda = 0.0423$  Å. In the integration,  $\mathbf{E}$  is evaluated as  $4\pi\mu/3$  if  $|\mathbf{E}|$  is larger than  $|4\pi\mu/3|$ , including the position of the dipole [31]. This is done for a few points very close to the dipole, i.e.,  $|\mathbf{r} - \mathbf{R}_{\text{dip}}| \sim 0.2$  Å. The pulse duration ( $T = 20$  fs) is short enough to avoid considering the nuclear dynamics and thus the ion position is fixed during the time evolution.

Before ending this section, we make comments on the validity of the theoretical model. We do not consider the self-consistent light matter interaction between the target molecule and radiation source. More specifically, we employ a theoretical model as in the case of the previous study in which the near-field is considered to be a radiation field from an oscillating dipole source and the back reaction of the electric field due to the target molecule on the source field is negligible. However, in the present theoretical model the size of the target molecule is relatively small and its induced dipole is not so strong. Thus, it can be reasonably assumed that the back reaction does not primarily affect the external source field. We need to explicitly take account of the back reaction when the target molecule becomes larger and its induced dipole is comparable with the oscillating dipole of the radiation source. The effect of the back reaction might be noticeable especially under the resonant condition and then should be treated by solving the Maxwell-Schrodinger coupled equation in a self-consistent manner. As mentioned in the beginning of this article, it is still computationally highly demanding to solve such a coupled equation in real nanostructure systems. In a model two-particle system, for instance, Govorov et al. discussed the effect of the back reaction [27].

#### 1.5.4 Optical Force on a Silver Nanoparticle

Figure 1.12 shows the time-dependent optical force exerted on the silver nanoparticle in the  $y$  direction calculated by Eq. (1.20) at (a)  $\omega = 1.0$  eV (off-resonance) and (b)  $\omega = 2.7$  eV (resonance) in the unit of aN. Figure 1.12(a) clearly shows that the optical force is biased so that  $F_y$  takes the positive value during the excitation. This means that the near-field induces an attractive force on the nanoparticle. On the other hand, under the resonance condition in Fig. 1.12(b)  $F_y$  takes both positive and negative values even though the force is also biased to the positive value. Focusing on the maximum values of  $F_y$  in these excitations, the resonantly induced optical force is slightly larger than the off-resonantly induced one. The time-averaged forces calculated by using Eq. (1.21) for each excitation are (a) 16.8 aN and (b) 16.9 aN. (As a reference, the gravitation acted on the nanoparticle is of the order of  $10^{-15}$  aN.)

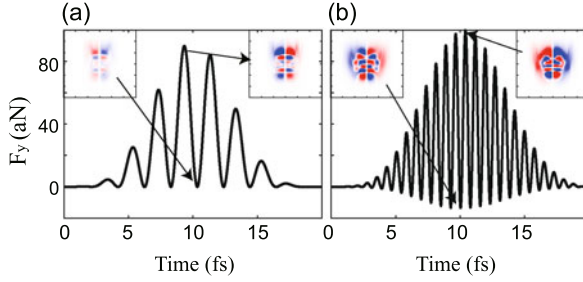


**Fig. 1.12** Time dependence of optical force on a silver particle exerted by the near-field at (a)  $\omega = 1.0$  eV (off-resonance) and (b) 2.7 eV (resonance). Insets are the snapshots of the induced electron densities where the red and the blue show increase and decrease in the electron density, respectively, compared to those of the ground state

This implies that the resonant condition does not necessarily significantly enhance the optical force.

The underlying mechanism of the near-field induced optical force on the nanoparticle can be schematically explained. As shown in Fig. 1.11, in the near-field region the electric field lines curve across the nanoparticle and the field intensity decreases with distance from the radiation source. When such a near-field is applied to the nanoparticle, polarization charges ( $\pm Q$ ) are induced in accordance with the curved electric-field-lines and the electron density distribution is biased, see the schematic of the induced charges in Fig. 1.13. In addition, the screening charges ( $\mp q$ ) are generated as counterparts of the polarization charges ( $\pm Q$ ). The terms of the polarization and screening charges were introduced to qualitatively explain the generation mechanism of the optical force. The computed results numerically take account of full contributions of these charges by solving the TDDFT calculations. Thus, the polarization and screening charges are not calculated separately and we cannot clearly distinguish one from the other. Then, the local effective force is exerted on the polarization and screening charges, depending on both their distributions and their signs of the charge. Similar optical response is commonly found in conventional photoinduced phenomena, irrespective of whether a uniform or nonuniform electric field is applied to a nanoparticle. However, oscillating uniform electric fields, which have frequently been used in the studies of optical response under the dipole approximation, exert no net force on a time average because the uniform (or symmetric) polarization and screening charges are induced. On the other hand, since the near-field is highly localized around a radiation source and the intensity of the field decreases rapidly with distance from the radiation source, net force is induced depending on intensity gradient of the near-field and on a balance between the amounts of the polarization and screening charges. In the present system, the force acting on the polarization charges (bold arrows in Fig. 1.13) is generally larger than on the screening charges (thin arrows). As a result, the near-field induced optical force is biased so that the attractive force ( $F_y > 0$ ) is exerted between the near-field fiber tip and the nanoparticle as shown in Fig. 1.12.

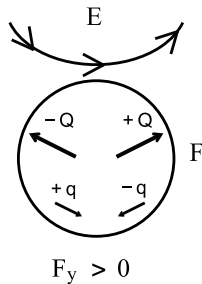


**Fig. 1.13** Scheme for the optical force due to the interaction between inhomogeneously induced charges and a near-field. The *top curve with arrows* shows the electric field, the *sphere* shows a nanoparticle, and  $Q$  and  $q$  are the polarization and screening charges, respectively. The *black arrows* indicate locally induced optical forces. The net optical force in the  $y$  direction is positive

The actual electron dynamics is more complicated. The four insets in Fig. 1.12 illustrate the snapshots of time evolution of the polarization and screening charges on the  $xy$  plane, where the red and the blue indicate increase and decrease in the electron density, respectively, compared to those of the initial ground state. The charge distributions are rather complex but appear to be somewhat regular in the sense that those nodal patterns are antisymmetric to the  $y$ -axis. Although it is difficult to clearly distinguish between the polarization and screening charges in the charge distribution, the snapshots of these charges are reminiscent of the schematic in Fig. 1.13. We computationally confirmed that in the resonance excitation (Fig. 1.12(b)) the polarization charges are induced in an inner region and the corresponding screening charges are localized around the nanoparticle surface. This is mainly because in the off-resonance excitation the electrons are forced to oscillate near the radiation source, whereas in the resonance excitation the specific electrons which are strongly associated with the details of the electronic structures primarily oscillate resonantly. Thus, in the resonance excitation the optical force partly becomes negative because the net force is determined by a balance between the amounts of the polarization and screening charges.

We next discuss the energy dependence of the optical force. Figure 1.14 shows the time-averaged force (red solid curve) and the absorption spectrum (black broken curve). The force spectrum was obtained by plotting the averaged optical force, varying the frequency by 0.1 eV from 0.8 to 3.6 eV. The absorption spectrum was obtained under a dipole approximation as in a similar way of previous methods. [32, 51]. The averaged force spectrum has peaks at 1.3 eV and 2.2 eV, which are different from the resonance frequency. Although the polarization charges are significantly induced when the laser frequency is in tune with the resonance frequency, this figure proves that the resonance excitation does not necessarily maximally induce the net force. This is because the screening charges partly (and sometimes largely) cancel the polarization charges. As a result of the sensible balance between the polarization and the screening charges, several maxima and minima appear in the force spectrum. Conversely, this result indicates that we can manipulate atoms and molecules in nanostructures by controlling the strength of attractive force (and

**Fig. 1.14** Absorption spectrum (*dashed curve*) of the silver nanoparticle and the time-averaged force on the particle as a function of energy

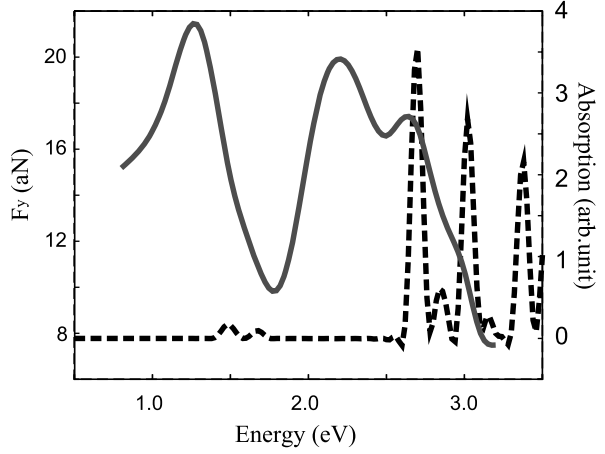
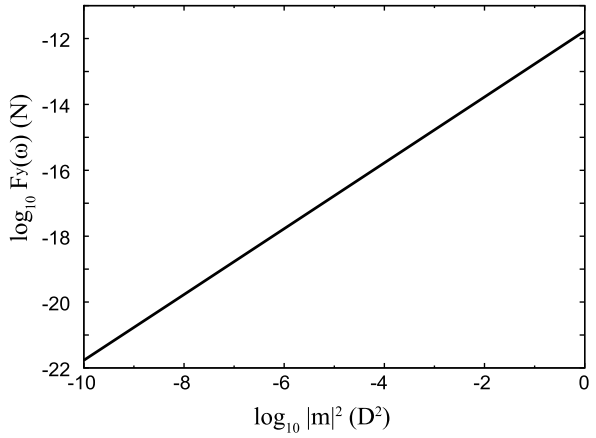


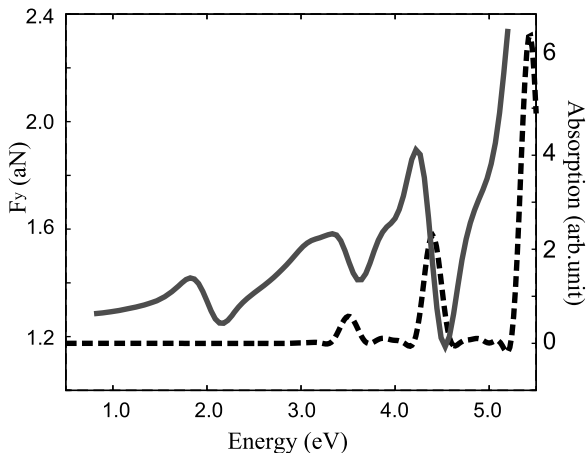
**Fig. 1.15** Time-averaged force on the silver particle under the off-resonant condition (1.0 eV) as a function of the square of the dipole moment of the radiation source



possibly repulsive force), changing the laser frequency. To do that, electronic structure calculations of target nanostructures must be carried out. Our electron dynamics approach combined with nonuniform light-matter interaction theory fulfills such a requirement.

Before discussing the results of  $C_{60}$ , we show the field-intensity dependence of the optical force. Since the present near-field is approximated by the oscillating dipole in the form of Eq. (1.22), we calculated the intensity dependence by varying the dipole moment of the radiating source, which is associated with the field intensity. The laser frequency  $\omega$  is set to 1.0 eV (off-resonance). Figure 1.15 shows the time-averaged optical force as a function of the square of the dipole moment of the radiation source. The  $x$  and  $y$  axes are shown in a logarithm scale with base 10. We found that the optical force is linearly proportional to the near-field intensity. The optical force amounts to  $10^{-12}$  N when the radiation source has the moment of 1D.

**Fig. 1.16** Same as Fig. 1.14  
but for  $C_{60}$



### 1.5.5 Optical Force on $C_{60}$

We have also calculated the optical force for  $C_{60}$  interacting with the near-field. Contrary to the case of the metal particle, the force on  $C_{60}$  does not become negative both for off-resonant (1 eV) and resonant (3.6 eV) conditions. This can be attributed to the hollow structure of  $C_{60}$  because there are no effective screening charges. The time-averaged forces are 1.29 aN (off-resonance condition) and 1.41 aN (resonance condition). In this case, stronger force is induced under the resonant condition than the off-resonant condition. The force on  $C_{60}$  is an order of magnitude smaller than that on the silver particle because of less mobility of the charges and of the absence of charges inside the sphere. We plot the time-averaged force (red solid curve) as a function of energy in Fig. 1.16. The absorption spectrum (black broken curve) is also drawn as a reference. The optical force has several peaks as similar to the force spectrum of the metal particle and generally increases as a function of the energy. The figure clearly demonstrates that the optical force is largely determined by the detailed electronic structures of the molecule.

### 1.5.6 Concluding Remarks

We have calculated the near-field induced optical forces acted on a silver particle mimicked by a jellium model and on  $C_{60}$ . The grid-based real-time and real-space time-dependent density functional theory approach combined with the nonuniform light-matter interaction formalism, recently developed by the authors, was employed to accurately calculate the inhomogeneous charge polarization induced by the full multipole interaction with the near-field. The induced force is rationally explained in terms of the polarization and screening charges. The local optical force on the silver particle in the  $y$  direction takes both positive and negative values depending

on the spatial distribution of these charges, and the net force becomes attractive as a result of a balance between the polarization and screening charges. The optical force on  $C_{60}$  is an order of magnitude smaller than that on the silver particle because of the less mobility of the electrons. The energy dependence of the optical force of these particles showed several maxima and minima, indicating that the resonance excitation does not necessarily induce the optical force most efficiently. Such a non-monotonic energy dependence of the optical force will be utilized when manipulating nanoparticles at the nanometer scale by controlling the near-field frequency. To calculate the optical forces induced by a highly nonuniform electric field in real molecules, a sensible balance of the polarization and screening charges must be determined. The present first-principles TDDFT approach taking account of full light-matter interactions can be a powerful tool for optical manipulation in nanostructures at the level of single atoms and molecules.

## 1.6 Summary

We have presented a generalized theoretical description of optical response in an effort to understand a nonuniform light-matter interaction between a near-field and a molecule. The present optical response theory fully taking account of the nonuniform light-matter interaction allows us to elucidate inhomogeneous electron dynamics associated with local electronic structures of a molecule at the 1 nm scale, even though the wavelength of an incident laser pulse is much longer than the size of the molecule. The near-field electron dynamics was computationally demonstrated for high-harmonic-generation and optical force. In contrast to a conventional electronic excitation process due to uniform light-matter interaction, the computed results illustrated unusual electron dynamics caused by the nonuniform light-matter interaction. We expect that the nonuniform light-matter interaction/TD-KS approach incorporated with the Maxwell equations will enable us to elucidate electron and electromagnetic field dynamics in nanostructures.

**Acknowledgements** This research was supported by a Grant-in-Aid (No. 21350018) and by the Next-Generation Supercomputer Project from the Ministry of Education, Culture, Sports, Science and Technology of Japan. The computation was partly performed at the Research Center for Computational Science, Okazaki, Japan.

## References

1. T.W. Ebbesen, H.J. Lezec, H.F. Ghaemi, T. Thio, P.A. Wolff, *Nature* **391**, 667 (1998)
2. K. Kobayashi, S. Sangu, H. Ito, M. Ohtsu, *Phys. Rev. A* **63**, 013806 (2001)
3. S.A. Maier, P.G. Kik, H.A. Atwater, S. Meltzer, E. Harel, B.E. Koel, A.A.G. Requicha, *Nat. Mater.* **2**, 229 (2003)
4. P.N. Prasad, *Nanophotonics* (Wiley-Interscience, New York, 2004)
5. C. Girard, *Rep. Prog. Phys.* **68**, 1883 (2005)

6. L. Novotny, B. Hecht, *Principles of Nano-Optics* (Cambridge University Press, Cambridge, 2006)
7. S.A. Maier, *Plasmonics: Fundamentals and Applications* (Springer, Berlin, 2007)
8. M. Fleischmann, P.J. Hendra, A.J. McQuillan, Chem. Phys. Lett. **26**, 163 (1974)
9. D.L. Jeanmaire, R.P. Van Duyne, J. Electroanal. Chem. **84**, 1 (1977)
10. M.G. Albrecht, J.A. Creighton, J. Am. Chem. Soc. **99**, 5215 (1977)
11. K. Imura, H. Okamoto, M.K. Hossain, M. Kitajima, Nano Lett. **6**, 2173 (2006)
12. D.W. Brandl, N.A. Mirin, P. Nordlander, J. Phys. Chem. B **110**, 12302 (2006)
13. J. Zhao, A.O. Pinchuk, J.M. McMahon, S. Li, L.K. Ausman, A.L. Atkinson, G.C. Schatz, Acc. Chem. Res. **41**, 1710 (2008). And references therein
14. M. Moskovits, Rev. Mod. Phys. **57**, 783 (1985)
15. K. Kneipp, M. Moskovits, H. Kneipp (eds.), *Surface-Enhanced Raman Scattering* (Springer, Heidelberg, 2006)
16. R. Aroca, *Surface-Enhanced Vibrational Spectroscopy* (Wiley, New York, 2006)
17. S. Nie, S.R. Emory, Science **275**, 1102 (1997)
18. K. Kneipp, Y. Wang, H. Kneipp, L.T. Perelman, I. Itzkan, R.R. Dasari, M.S. Feld, Phys. Rev. Lett. **78**, 1667 (1997)
19. T. Vo-Dinh, K. Houck, D.L. Stokes, Anal. Chem. **66**, 3379 (1994)
20. Y.C. Cao, R. Jin, C.A. Mirkin, Science **297**, 1536 (2002)
21. K. Cho, Prog. Theor. Phys. Suppl. 225–233 (1991)
22. J.K. Jenkins, S. Mukamel, J. Chem. Phys. **98**, 7046 (1993)
23. O. Keller, Phys. Rep. **268**, 85 (1996)
24. D. Abramavicius, S. Mukamel, J. Chem. Phys. **124**, 034113 (2006)
25. K. Lopata, D. Neuhauser, R. Baer, J. Chem. Phys. **127**, 154714 (2007)
26. E. Lorin, S. Chelkowski, A. Bandrauk, Comput. Phys. Commun. **177**, 908 (2007)
27. J.Y. Yan, W. Zhang, S.Q. Duan, X.G. Zhao, A.O. Govorov, Phys. Rev. B **77**, 165301 (2008)
28. K. Lopata, D. Neuhauser, J. Chem. Phys. **130**, 104707 (2009)
29. C. Cohen-Tannoudji, J. Dupont-Roc and, G. Grynberg, *Photons and Atoms—Introduction to Quantum Electrodynamics* (Wiley-Interscience, New York, 1989)
30. D.P. Craig, T. Thirunamachandran, *Molecular Quantum Electrodynamics* (Dover, New York, 1998)
31. S. Mukamel, *Principles of Nonlinear Optical Spectroscopy*. Oxford Series on Optical and Imaging Sciences (Oxford University Press, London, 1999)
32. K. Yabana, G.F. Bertsch, Phys. Rev. B **54**, 4484 (1996)
33. K. Nobusada, K. Yabana, Phys. Rev. A **70**, 043411 (2004)
34. K. Shiratori, K. Nobusada, K. Yabana, Chem. Phys. Lett. **404**, 365 (2005)
35. K. Nobusada, K. Yabana, Phys. Rev. A **75**, 032518 (2007)
36. J.D. Jackson, *Classical Electrodynamics*, 3rd edn. (Wiley, New York, 1998)
37. E. Runge, E.K.U. Gross, Phys. Rev. Lett. **52**, 997 (1984)
38. F. Calvayrac, P.G. Reinhard, E. Suraud, C.A. Ullrich, Phys. Rep. **337**, 493 (2000)
39. M.A.L. Marques, A. Castro, G.F. Bertsch, A. Rubio, Comput. Phys. Commun. **151**, 60 (2003)
40. N. Troullier, J.L. Martins, Phys. Rev. B **43**, 1993 (1991)
41. L. Kleinman, D.M. Bylander, Phys. Rev. Lett. **48**, 1425 (1982)
42. J.P. Perdew, A. Zunger, Phys. Rev. B **23**, 5048 (1981)
43. I. Vasiliev, S. Ogut, J.R. Chelikowsky, Phys. Rev. B **65**, 115416 (2002)
44. A. Wasserman, N.T. Maitra and, K. Burke, Phys. Rev. Lett. **91**, 263001 (2003)
45. G.F. Gabriele, G. Vignale, *Quantum Theory of the Electron Liquid* (Cambridge University Press, Cambridge, 2005)
46. F. Cataldo, Polyhedron **23**, 1889 (2004)
47. TURBOMOLE Version 5.10, Quantum Chemistry Group, University of Karlsruhe, Karlsruhe, Germany (2008)
48. R. Ahlrichs, M. Bär, M. Häser, H. Horn, C. Kölmel, Chem. Phys. Lett. **162**, 165 (1989)
49. J.P. Perdew, Y. Wang, Phys. Rev. B **45**, 13244 (1992)
50. A. Schäfer, H. Horn, R. Ahlrichs, J. Chem. Phys. **97**, 2571 (1992)

51. K. Yabana, G.F. Bertsch, *Int. J. Quant. Chem.* **75**, 55 (1999)
52. J.R. Chelikowsky, N. Troullier, K. Wu, Y. Saad, *Phys. Rev. B* **50**, 11355 (1994)
53. K. Burnett, V.C. Reed, J. Cooper, P.L. Knight, *Phys. Rev. A* **45**, 3347 (1992)
54. T. Brabec, F. Krausz, *Rev. Mod. Phys.* **72**, 545 (2000)
55. S. Tojo, M. Hasuo, *Phys. Rev. A* **71**, 012508 (2005)
56. J.J. Sakurai, *Modern Quantum Mechanics* (Addison-Wesley, Reading, 1993) (revised edition)
57. R.W. Boyd, *Nonlinear Optics*, 3rd edn. (Academic Press, San Diego, 2008)
58. C.T. Lee, W.T. Yang, R.G. Parr, *Phys. Rev. B* **37**, 785 (1988)
59. A.D. Becke, *J. Chem. Phys.* **98**, 5648 (1993)
60. A. Ashkin, *Phys. Rev. Lett.* **24**, 156 (1970)
61. A. Ashkin, J.M. Dziedzic, J.E. Bjorkholm, S. Chu, *Opt. Lett.* **11**, 288 (1986)
62. A. Ashkin, *IEEE J. Sel. Top. Quantum Electron.* **6**, 841 (2000)
63. D.G. Grier, *Nature* **424**, 810 (2003)
64. K.C. Neuman, S.M. Block, *Rev. Sci. Instrum.* **75**, 2787 (2004)
65. J.C. Crocker, D.G. Grier, *Phys. Rev. Lett.* **77**, 1897 (1996)
66. B. Lin, J. Yu, S.A. Rice, *Colloids Surf. A* **174**, 121 (2000)
67. K. Svoboda, S.M. Block, *Annu. Rev. Biophys. Biomol. Struct.* **23**, 247 (1994)
68. U. Seifert, *Adv. Phys.* **46**, 13 (1997)
69. A.D. Mehta, M. Rief, J.A. Spudich, D.A. Smith, R.M. Simmons, *Science* **283**, 1689 (1999)
70. M.J. Lang, S.M. Block, *Am. J. Phys.* **71**, 201 (2003)
71. L. Novotny, R.X. Bian, X.S. Xie, *Phys. Rev. Lett.* **79**, 645 (1997)
72. E. Lorin, S. Chelkowski, A. Bandrauk, *Comput. Phys. Commun.* **177**, 908 (2007)
73. K. Lopata, D. Neuhauser, *J. Chem. Phys.* **130**, 104707 (2009)
74. K. Okamoto, S. Kawata, *Phys. Rev. Lett.* **83**, 4534 (1999)
75. P.C. Chaumet, M. Nieto-Vesperinas, *Phys. Rev. B* **61**, 14119 (2000)
76. A.I. Bishop, T.A. Nieminen, N.R. Heckenberg, H. Rubinsztein-Dunlop, *Phys. Rev. A* **68**, 033802 (2003)
77. T. Iida, H. Ishihara, *Phys. Rev. Lett.* **90**, 057403 (2003)
78. V. Wong, M.A. Ratner, *Phys. Rev. B* **73**, 075416 (2006)
79. T. Iwasa, K. Nobusada, *Phys. Rev. A* **80**, 043409 (2009)
80. N.W. Ashcroft, N.D. Mermin, *Solid State Physics* (Brooks/Cole Thomson Learning, Pacific Grove, 1976)



Progress in Nanophotonics 2

Ohtsu, M. (Ed.)

2013, XIII, 169 p. 144 illus., 32 illus. in color., Hardcover

ISBN: 978-3-642-35718-3